REPORT DOCUMENTATION PAGE

2

Form Approved OMB NO. 0704-0188

1. REPORT DATE (DD-MM-YYYY)	2. REPORT TYPE	3. DATES COVERED (From - To)
	New Reprint	-

4. TITLE AND SUBTITLE

Stability and degradation mechanisms of metal–organic frameworks containing the Zr6O4(OH)4 secondary building unit

5a. CONTRACT NUMBER

W911NF-10-1-0076

5b. GRANT NUMBER

5c. PROGRAM ELEMENT NUMBER

622622

6. AUTHORS

Jared B. DeCoste, Gregory W. Peterson, Himanshu Jasuja, T. Grant Glover, You-gui Huang, Krista S. Walton

5d. PROJECT NUMBER

5e. TASK NUMBER

5f. WORK UNIT NUMBER

7. PERFORMING ORGANIZATION NAMES AND ADDRESSES

Georgia Tech Research Corporation
505 Tenth Street NW

Atlanta, GA 30332 -0420

8. PERFORMING ORGANIZATION REPORT NUMBER

9. SPONSORING/MONITORING AGENCY NAME(S) AND ADDRESS (ES)

U.S. Army Research Office
P.O. Box 12211
Research Triangle Park, NC 27709-2211

10. SPONSOR/MONITOR'S ACRONYM(S)

ARO

11. SPONSOR/MONITOR'S REPORT NUMBER(S)

57994-CH.26

12. DISTRIBUTION AVAILIBILITY STATEMENT

Approved for public release; distribution is unlimited.

13. SUPPLEMENTARY NOTES

The views, opinions and/or findings contained in this report are those of the author(s) and should not contrued as an official Department of the Army position, policy or decision, unless so designated by other documentation.

14. ABSTRACT

See publication.

15. SUBJECT TERMS

MOF stability

16. SECURITY CLASSIFICATION OF:			17. LIMITATION OF ABSTRACT	15. NUMBER OF PAGES	19a. NAME OF RESPONSIBLE PERSON
a. REPORT	b. ABSTRACT	c. THIS PAGE			Krista Walton
UU	UU	UU	UU		19b. TELEPHONE NUMBER: 404-894-5254

Report Title

Stability and degradation mechanisms of metal–organic frameworks containing the Zr6O4(OH)4 secondary building unit

ABSTRACT

See publication.

REPORT DOCUMENTATION PAGE (SF298)
(Continuation Sheet)

Continuation for Block 13

ARO Report Number 57994.26-CH
Stability and degradation mechanisms of metal–...

Block 13: Supplementary Note

Approved for public release; distribution is unlimited.

Journal of Materials Chemistry A

RSC Publishing

PAPER

View Article Online
View Journal | View Issue

Cite this: J. Mater. Chem. A, 2013, 1, 5642

Stability and degradation mechanisms of metal–organic frameworks containing the $Zr_6O_4(OH)_4$ secondary building unit†

Jared B. DeCoste,*[a] Gregory W. Peterson,[b] Himanshu Jasuja,[c] T. Grant Glover,[a] You-gui Huang[c] and Krista S. Walton[c]

Received 13th February 2013
Accepted 15th March 2013

DOI: 10.1039/c3ta10662d

www.rsc.org/MaterialsA

Metal–organic frameworks (MOFs) with the $Zr_6O_4(OH)_4$ secondary building unit (SBU) have been of particular interest for potential commercial and industrial uses because they can be easily tailored and are reported to be chemically and thermally stable. However, we show that there are significant changes in chemical and thermal stability of $Zr_6O_4(OH)_4$ MOFs with the incorporation of different organic linkers. As the number of aromatic rings is increased from one to two in 1,4-benzene dicarboxylate (UiO-66, ZrMOF–BDC) and 4,4′-biphenyl dicarboxylate (UiO-67, ZrMOF–BPDC), the $Zr_6O_4(OH)_4$ SBU becomes more susceptible to chemical degradation by water and hydrochloric acid. Furthermore, as the linker is replaced with 2,2′-bipyridine-5,5′-dicarboxylate (ZrMOF–BIPY) the chemical stability decreases further as the MOF is susceptible to chemical breakdown by protic chemicals such as methanol and isopropanol. The results reported here bring into question the superior structural stability of the UiO-67 analogs as reported by others. Furthermore, the degradation mechanisms proposed here may be applied to other classes of MOFs containing aromatic dicarboxylate organic linkers, in order to predict their structural stability upon exposure to solvents.

Introduction

Metal–organic frameworks (MOFs) have been of particular interest in the areas of gas storage,[1] catalysis,[2] molecular sensing,[3,4] and toxic gas filtration.[5,6] MOFs are able to be tailored for targeted chemical interaction through variation of functional groups attached to the organic linker as in the isoreticular MOF (IRMOF) series,[7] or the metal in the secondary building unit (SBU) as with MOF-74 analogs.[5] However, one of the major deterrents to being used in industrial or commercial applications is the instability of many carboxylate containing MOFs in the presence of liquid water or high humidity.[8]

Many have investigated methods for modifying MOFs to increase their stability, but very few have investigated the driving forces behind the chemical stability/instability of certain MOFs. Tan *et al.*, examined the hydrolysis mechanisms causing the instability of $M(BDC)(DABCO)_{0.5}$ [M = Cu, Zn, Ni, Co] (DMOF). They found that the metal incorporated in the MOF has an effect on the stability, and breakdown mechanism. A hydrolysis reaction of water molecules with the Cu–O–C is observed in the case of Cu–DMOF, while displacement of DABCO linkers by water occurs in Zn– and Co–DMOF. However, Ni–DMOF was shown to be less susceptible to hydrolysis.[9]

Cu–BTC (HKUST-1), a highly water unstable MOF, has been stabilized in the presence of water through a plasma enhanced chemical vapor deposition of perfluorohexane, leading to a super-hydrophobic MOF that can float on water.[10] IRMOF-1 (MOF-5) has been shown to have an enhancement in moisture resistance upon thermal treatment, by creating a carbonaceous outer coating around the MOF; however, the increased hydrophobicity is at the expense of surface area and functionality.[11] IRMOF-1 has also been shown to have its hydrostability increased through doping with Ni^{2+} ions during synthesis.[12] DMOF has been shown to be able to have its water stability tuned through the incorporation of various pendant groups on the benzene dicarboxylate linker.[13,14] Non-polar shielding groups, such as methyl groups, on the linker were shown to enhance the water stability of the MOF.

It is ideal for MOFs to have inherent water stability, as to which no post-synthetic modification is necessary. Beyond many of the techniques for enhancing water stability being labor and resource intensive, they can also alter the physical and chemical properties of the MOF.[10–14] Lillerud *et al.* reported UiO-66, a MOF with both high chemical and thermal stability.[15]

[a]Science Applications International Corporation (SAIC), Inc., PO Box 68, Gunpowder, MD 21010, USA. E-mail: jared.b.decoste2.ctr@mail.mil

[b]Edgewood Chemical Biological Center, 5183 Blackhawk Rd, Aberdeen Proving Ground, MD 21010, USA

[c]Georgia Institute of Technology, School of Chemical and Biomolecular Engineering, 211 Ferst Drive NW, Atlanta, GA 30332, USA

† Electronic supplementary information (ESI) available. See DOI: 10.1039/c3ta10662d

The UiO series of MOFs is defined by the $Zr_6O_4(OH)_4$ SBU, which is twelve-coordinated to 1,4-benzene dicarboxylate ligands in UiO-66, and biphenyl-4,4′-dicarboxylate ligands in UiO-67. It is reported that the SBU is the key to the exceptional stability, and has the ability to reversibly change between a hydroxylated ($Zr_6O_4(OH)_4$) and a dehydroxylated (Zr_6O_6) structure. Lillerud *et al.* states in multiple manuscripts that the UiO series of MOFs including UiO-66, UiO-67, and many UiO-66 analogs with varying pendant groups are all stable to aqueous and acidic conditions; however, there is a lack of evidence in way of experimental results to actually make such universal claims for all UiO MOFs.[15–17] In fact, it has been reported by others that UiO-67 is not as stable in liquid water as UiO-66, but no insight into the reasoning why this is the case has been given.[18]

Many analogs that are isostructural to UiO-66 can be synthesized through similar synthesis procedures to those of UiO-66. Pendant groups of varying electronic properties, including –Br, $–NH_2$, and $–NO_2$, can be directly incorporated onto the aromatic ring of terephthalic acid and subsequently into the MOF through direct synthesis.[17,19] Furthermore, the UiO-66–NH_2 analog can be post-synthetically modified with anhydrides to form amide functional groups.[19] UiO-66 analogs with one and two (*para* to one another) alkyl groups bound to the terephthalic acid ligand have also been synthesized, and shown to have similar physical and chemical properties to those of UiO-66.[20,21]

Cohen *et al.* reported the ability of functionalizing UiO-66 analogs through a post-synthetic ligand and cation exchange.[22–24] The ability of UiO-66 analogs to exchange readily in aqueous environments suggests that the structure is not as chemically inert as first suggested by Lillerud *et al.*[15] In an aqueous solution of terephthalic acid analogs, UiO-66 can readily exchange its linker with a linker in solution. The degree of exchange at equilibrium can be controlled by the temperature of the solution.[22] Furthermore, the Zr atoms in the SBU can be exchanged for Ti or Hf utilizing a proper M^{4+} source.[24] This is the first known incorporation of Ti into a M_6O_6 SBU; however, the Hf analog of UiO-66 has been synthesized directly from $HfCl_4$ and terephthalic acid.[25]

In this work, we investigate in depth the thermal and chemical stability of the UiO series of MOFs through nitrogen and water isotherms, thermogravimetric analysis, powder X-ray diffraction, and attenuated total reflectance Fourier transform infrared spectroscopy. Four zirconium MOFs (ZrMOFs) were synthesized varying only the organic linker of terephthalate to 2-aminoterephthalate, biphenyl-4,4′-dicarboxylate, and 2,2′-bipyridine-5,5′-dicarboxylate. These four ZrMOFs represent the base UiO-66, UiO-66 with an amine functional group, UiO-67, and UiO-67 with nitrogen atoms for possible ligation of metal ions.[26] To the best of the knowledge of the authors, the bipyridine functionalized ZrMOF has not been reported in the literature to date. These MOFs were subjected to a variety of chemicals that represent common conditions in industrial processes, solvent exchange, and/or in laboratory experiments. It is important to fully understand the thermal and chemical stability of any material that may be used in these processes. The selection of water, methanol, isopropanol, acetone, pyridine, chloroform, hydrogen chloride, and sodium hydroxide represent a wide range of chemistries as well as industrial uses. These chemicals lend insight into the breakdown mechanisms of each ZrMOF and will allow one to predict the stability of other ZrMOFs in a variety of chemicals.

Experimental

Synthesis

All chemicals were obtained from Sigma Aldrich and used without further purification. A scaled up variation of the synthetic procedure used by Lillerud *et al.* was used to synthesize each ZrMOF varying only the organic linker used.[15] $ZrCl_4$ (150 mg, 0.641 mmol) and the organic linker (terephthalic acid, 106 mg, 0.641 mmol; 2-aminoterephthalic acid, 116 mg, 0.641 mmol; biphenyl-4,4′-dicarboxylic acid, 155 mg, 0.641 mmol; or 2,2′-bipyridine-5,5′-dicarobylxic acid, 157 mg, 0.641 mmol, structures of the organic linkers used are shown in Fig. 1) were dissolved in 10 mL of DMF at room temperature. The mixture was sealed in a 20 mL scintillation vial and heated to 120 °C for 24 h. The resulting solid was filtered and washed with DMF. The MOFs synthesized resulted in ZrMOF–BDC (UiO-66), ZrMOF–NH_2, ZrMOF–BPDC (UiO-67), and ZrMOF–BIPY respectively.

Chemical stability

Approximately 25 mg of each ZrMOF was placed in vials containing 5 mL of H_2O, 0.1 M HCl, 0.1 M NaOH, methanol, isopropanol, chloroform, pyridine, and acetone. Samples were allowed to sit statically at room temperature for 24 h. The samples were filtered and the solid was recovered for analysis.

Thermogravimetric analysis

Approximately 10 mg of each ZrMOF sample was loaded into a platinum pan for analysis with a TA Instruments Q 500 thermogravimetric analyzer (TGA). The temperature of the samples was raised from room temperature to 800 °C at a rate of 5 °C min^{-1} under a constant flow of zero air at 20 mL min^{-1}. The mass of the sample was recorded at a rate of 0.5 s per scan.

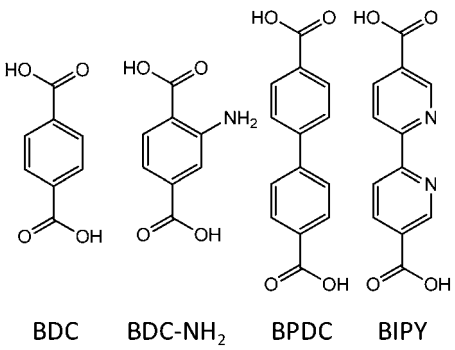

Fig. 1 ZrMOF syntheses use 1,4-benzene dicarboxylic acid, 2-aminoterephthalic acid, biphenyl-4,4′-dicarboxylic acid, and 2,2′-bipyridine-5,5′-dicarboxylic acid (left to right) as organic linkers in ZrMOF–BDC, ZrMOF–NH_2, ZrMOF–BPDC, and ZrMOF–BIPY respectively.

BET analysis

BET modeling of nitrogen adsorption isotherms measured at 77 K was performed to obtain the specific surface areas ($m^2 g^{-1}$). The BET model was applied over the pressure range as described by Walton and Snurr to obtain physically meaningful parameters.[27] Nitrogen adsorption isotherms were measured for each activated MOF sample before and after water exposure using a Quadrasorb SI analyzer from Quantachrome Instruments. All the MOFs mentioned in this study were activated overnight (at 150 °C under vacuum) prior to the run and approximately 20–30 mg sample size was used.

Water vapor isotherms

Water vapor isotherm measurements were carried out at 25 °C and 1 bar using an IGA-3 series gravimetric adsorption apparatus from Hiden Analytical Ltd. Prior to the run, approximately 20–35 mg sample sizes were loaded into the IGA-3 device followed by *in situ* activation (at 150 °C under vacuum) until no further weight loss was observed. To mimic real humid environment conditions, dry air was chosen as the carrier gas. A portion of the carrier gas was bubbled through a canister filled with deionized water. Two mass flow controllers were used to vary the ratio of saturated air to dry air so that desired relative humidity (RH) can be achieved. Water adsorption experiments were conducted up to 90% RH with total gas flow rate of 200 $cm^3 min^{-1}$ and typical equilibrium times ranging from 15 min to 24 h for each point in the adsorption isotherm. Water exposed samples were reactivated (at 150 °C under vacuum) to calculate the loss in BET surface area.

Powder X-ray diffraction

Each ZrMOF was analyzed using powder X-ray diffraction (PXRD) pre and post chemical and thermal exposure. PXRD measurements were taken using a PANalytical X'Pert X-ray powder diffractometer with an X'celerator detector. Samples were scanned at 45 kV and 40 mA, using Cu Kα radiation (λ = 1.54 Å), a step size of $2\theta = 0.033°$ (10.08 s per step) over the applicable 2θ range. Zero-background discs were used to minimize background scattering. PXRD diffraction patterns were processed using the Reflex module in Material Studio 6.0 by Accelrys.

Attenuated total reflectance Fourier transform infrared spectroscopy

Attenuated total reflectance Fourier transform infrared spectroscopy (ATR-FTIR) spectra of the ZrMOFs before and after chemical exposure were taken using a Bruker Tensor 27 FTIR with a Bruker Platinum ATR accessory equipped with a single reflection diamond crystal. Sixteen scans were averaged over a range of 4000 to 600 cm^{-1} with a resolution of 4 cm^{-1}.

Results and discussion

Thermal stability of ZrMOFs

Each ZrMOF was confirmed by PXRD to have the structures reported in the literature as can be seen in Fig. 2.[15,16] The PXRD patterns show that ZrMOF–BDC and ZrMOF–NH_2 are isostructural to one another with similar unit cell sizes; the same holds true for ZrMOF–BPDC and ZrMOF–BIPY. We believe this to be the first known report of the bipyridine analog of UiO-67.

The TGA results are illustrated in Fig. 3. ZrMOF–BDC and ZrMOF–BPDC have similar thermal decomposition temperatures of ~520 °C, which is in accordance with literature values.[15] The ZrMOF–BIPY has a lower thermal decomposition

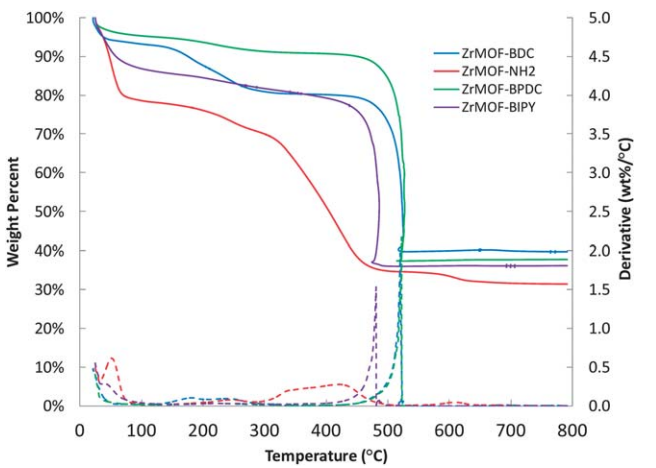

Fig. 3 TGA data shows the weight loss of ZrMOF–BDC (blue), ZrMOF–NH_2 (red), ZrMOF–BPDC (green) and ZrMOF–BIPY (purple) of the range of 25 to 800 °C. The derivative of the weight loss with respect to temperature is depicted by dashed lines.

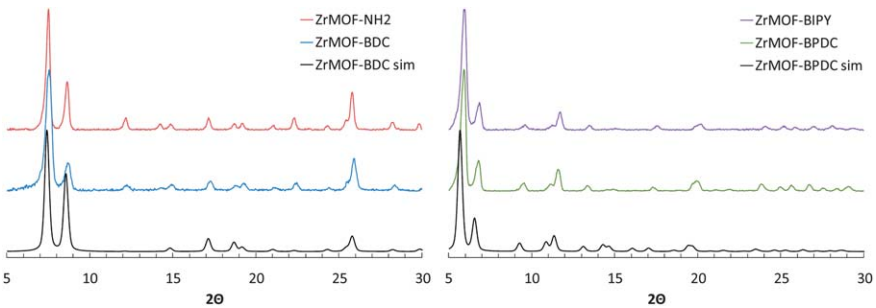

Fig. 2 PXRD patterns of ZrMOF–BDC (simulated and experimental), ZrMOF–NH_2 (experimental), ZrMOF–BPDC (simulated and experimental), and ZrMOF–BIPY (experimental).

temperature of ~480 °C. ZrMOF–NH_2 did not have as sharp of a degradation step as the other ZrMOFs, occurring over the range of 300 to 500 °C. Kandiah *et al.* showed with temperature dependant XRD that over this range the crystallinity of ZrMOF–NH_2 changed gradually as the structure broke down.[17] The ability of the nitrogen atoms to withdraw electrons inductively weakens the neighboring carbon–carbon bonds, causing thermal breakdown of ZrMOFs at lower temperatures in ZrMOF–NH_2 and ZrMOF–BIPY.

A separate experiment was done where each ZrMOF was heated in air at 350, 550, and 800 °C for 120 minutes to determine the steps of thermal degradation. The resulting powders were analyzed using PXRD as can be seen in Fig. 4. As reported by others, the initial bond breaking that occurs upon thermal treatment for ZrMOFs is not the coordinative covalent bonds between the linker and the SBU, but instead the carbon–carbon bond between the benzene ring and the carboxylate carbon.[15,17] All samples except ZrMOF–NH_2 are shown to be structurally stable to 350 °C; at this temperature ZrMOF–NH_2 is shown to be amorphous. At temperatures of 550 °C, each ZrMOF shows the appearance of peaks at $2\Theta \approx 30.5$ and 35.0°, which are indicative of the (111) and the (200) planes of tetragonal zirconia respectively. As the temperature is raised to 800 °C, more well defined peaks appear at $2\Theta \approx 28.2$, 31.6, 34.7, and 35.3°, which are indicative of the $(11\bar{1})$, (111), (020), and (200) planes of monoclinic zirconia respectively.[28] The transition from an amorphous phase to the tetragonal phase and finally to the monoclinic phase with increasing temperature is typical for hydrated Zr^{4+} polycations, similar to those found in ZrMOFs.[28,29] As the temperature is increased, an increase in crystallization occurs condensing bridging and/or terminal Zr–OH groups into ZrO_2 sheets.[30]

Water vapor isotherms of ZrMOFs

The water isotherm measured at 298 K for each ZrMOF can be seen in Fig. 5. It is interesting to note the decreased uptake of water for ZrMOF–BPDC and –BIPY, when compared to ZrMOF–BDC and –NH_2. It would be expected for the double ring linkers of ZrMOF–BPDC and –BIPY to exhibit an increase in water uptake as the surface area and pore volumes are increased. This can be explained by examining the BET surface area of each material before and after the water isotherm experiment, as can be seen in Table 1. The BET surface areas of ZrMOF–BDC and –BPDC before the water isotherm experiment are consistent with the values reported in the literature.[16] The decrease in specific surface area for ZrMOF–NH_2, when compared to ZrMOF–BDC, is expected due to the increased mass of each linker without a significant increase in available N_2 adsorption sites. The increase in surface area for ZrMOF–BIPY, when compared to ZrMOF–BPDC, is slightly more difficult to explain, but very few in the literature have been able to approach the theoretical surface area of 2850 $m^2\ g^{-1}$ for ZrMOF–BPDC.[16] This may be due to the instability of these structures under conditions of relatively high humidity, as was seen by the near total loss of surface area of ZrMOF–BPDC and –BIPY after the water

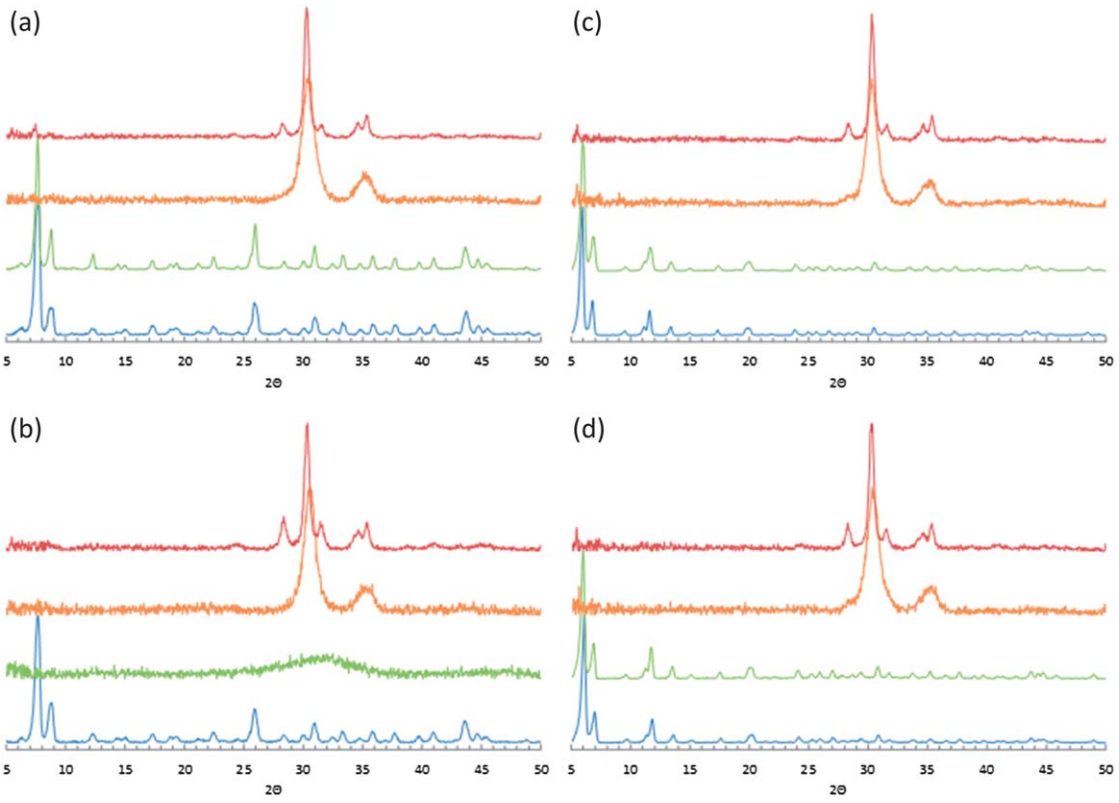

Fig. 4 PXRD spectra from $2\Theta = 5$ to 50° of (a) ZrMOF–BDC, (b) ZrMOF–NH_2, (c) ZrMOF–BPDC, and (d) ZrMOF–BIPY as synthesized (blue) and after heating to 350 °C (green), 550 °C (orange), and 800 °C (red) for 2 hours in air.

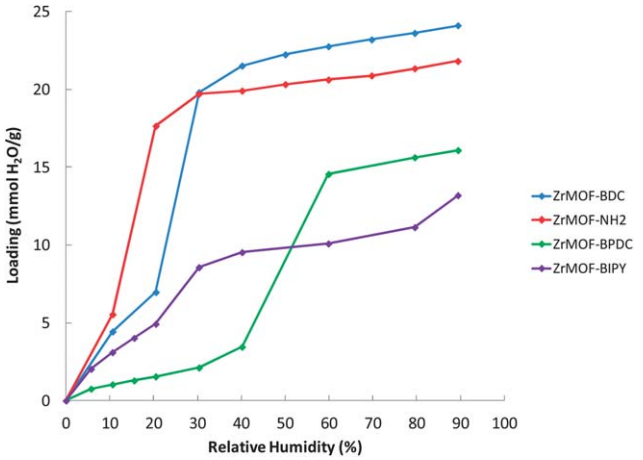

Fig. 5 Water vapor isotherms of ZrMOF–BDC (blue), –NH_2 (red), –BPDC (green) and –BIPY (purple) measured from 0 to 90% RH at 298 K.

Table 1 The measured BET surface area before and after taking the water vapor isotherm at 25 °C for ZrMOF–BDC, –NH_2, –BPDC, and –BIPY

	BET Surface area ($m^2\ g^{-1}$)	
Sample description	Pre-exposure	Post-exposure
ZrMOF–BDC	1080	1080
ZrMOF–NH_2	1005	1015
ZrMOF–BPDC	2145	10
ZrMOF–BIPY	2385	10

isotherm experiments. The post water isotherm XRD patterns of these structures show near total loss of crystallinity, as can be seen in Fig. S1–S4.†

The water isotherm for ZrMOF–NH_2 shows micropore filling occurring at relative humidity levels less than 20%, while ZrMOF–BDC does not show micropore filling until relative humidity levels of 30% are reached. This is due to the increased degree of intermolecular forces from the ability of water to hydrogen bond with the –NH_2 group in ZrMOF–NH_2. This phenomenon can also be seen for ZrMOF–BIPY when compared to ZrMOF–BPDC, albeit these structures exhibit micropore filling at much higher relative humidity levels when compared to the single ring ZrMOFs, due to the increased pore size. These results are consistent with those observed by Shoenecker *et al.* for ZrMOF–BDC and –NH_2, who also noted that a hysteresis in the desorption step of the water isotherms for the ZrMOFs is likely due to the rehydroxylation of the 7-coordinated inorganic brick to an 8-coordinated species.[31,32]

Chemical stability of ZrMOFs

The XRD pattern (from $2\Theta = 5$ to 30°) of each ZrMOF exposed to neat water, methanol, isopropanol, acetone, pyridine, chloroform, 0.1 M NaOH and 0.1 M HCl for 24 h can be seen in Fig. 6. These chemicals represent common solvents used in MOF solvent exchange or post-synthetic modifications, as well as common processing chemicals for industrial processes. Each ZrMOF has unique chemical stability and is not identical to ZrMOF–BDC as indicated by Lillerud *et al.*[15] ZrMOF–BDC shows structural stability towards all chemicals in this study, with the exception of 0.1 M NaOH. The breakdown in the presence of NaOH produced an amorphous XRD pattern. The XRD patterns for ZrMOF–NH_2 show similar results as ZrMOF–BDC, only showing structural breakdown for 0.1 M NaOH.

ZrMOFs with double ring linkers are shown to have decreased chemical stability when compared to the single ring linkers. ZrMOF–BPDC shows structural breakdown when exposed to water, 0.1 M HCl and 0.1 M NaOH. While the breakdown in the presence of NaOH shows an amorphous structure, HCl and water show the presence of new XRD peaks. These peaks are in good agreement with the XRD pattern of monoclinic zirconia. The peaks at $2\Theta \approx 17.5$, 25.1, and 28.0° represent the (100), (110), and $(11\bar{1})$ planes respectively.[33]

ZrMOF–BIPY shows significant structural breakdown when exposed to water, methanol, isopropanol, 0.1 M HCl, and 0.1 M NaOH. Furthermore some breakdown may be occurring upon exposure to acetone and chloroform, as evidenced by the presence of monoclinic ZrO_2 peaks in the XRD patterns. It should be noted here that each protic chemical studied (*i.e.* methanol, isopropanol, and water) was shown to breakdown the structure of ZrMOF–BIPY. This is consistent with the ability of the nitrogen atoms on the 2,2′-bipyridine-5,5′-dicarboxylic acid to act as a base and remove the proton from protic chemicals. Water, methanol, and isopropanol are transformed into hydroxide, methoxy, and isopropoxy anions respectively upon deprotonation. These strong nucleophiles can attack the ZrMOF structure and structural breakdown occurs. Furthermore, the breakdown of the structure by HCl and NaOH is similar to that seen in the ZrMOF–BPDC.

The ATR-FTIR spectra from 1800 to 600 cm^{-1} of each ZrMOF post exposure to each chemical studied can be seen in Fig. 7. Many of the stretches for ZrMOF–BDC and ZrMOF–BPDC have been assigned by others.[16,34] Stretches at ~1652, 1254, 1100, and 1062 cm^{-1} represent the vibrational modes of the DMF used in the synthesis of each ZrMOF. The distinguishing characteristics for ZrMOF–NH_2 from ZrMOF–BDC are the N–H scissoring vibration at 1626 cm^{-1} and the strong aromatic C–N stretch at 1356 cm^{-1}. The differences between ZrMOF–BIPY and ZrMOF–BPDC are much greater due to the incorporation of a nitrogen atom directly into the ring. The ring modes have shifted from stretches at ~1501, 1408, 1269, 1179, and 1153 cm^{-1} for ZrMOF–BPDC to ~1473, 1409, 1283, 1245, 1164, and 1123 cm^{-1} for ZrMOF–BIPY.[35] Appropriate infrared stretches in each ZrMOF were confirmed to be part of the organic linker through ATR-FTIR of the neat organic linkers used in the ZrMOF synthesis, as can be seen in Fig. S5.†

ZrMOF–BDC shows little evidence of chemical breakdown in the presence of any of the chemicals investigated, with the exception of HCl, and NaOH. The changes in the FTIR spectrum for NaOH were expected due to the complete change in the XRD pattern; however, there was not as much evidence for the chemical change in the presence of HCl in the XRD pattern. Upon closer investigation it can be seen in the HCl exposed ZrMOF–BDC XRD pattern that there is a decrease to the signal-to-noise

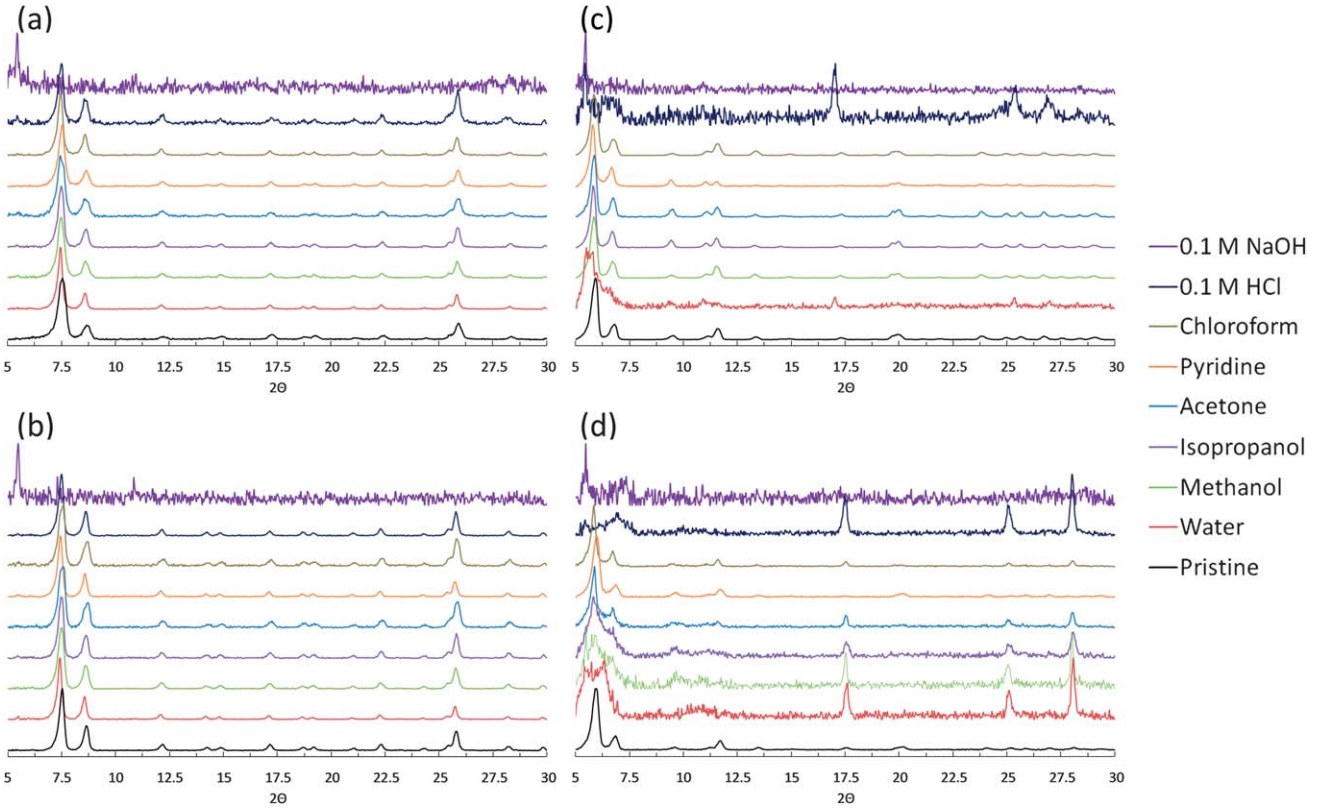

Fig. 6 PXRD spectra from $2\Theta = 5$ to 30° of (a) ZrMOF–BDC, (b) ZrMOF–NH_2, (c) ZrMOF–BPDC, and (d) ZrMOF–BIPY as synthesized and after exposure to a variety of chemicals.

and a small peak rising from the baseline at $2\Theta \sim 5.5°$, which is seen in many of the other XRD patterns that exhibit structural breakdown. The FTIR spectrum of HCl exposed ZrMOF–BDC shows most of the same bands that are seen in the pristine sample; however, there is the presence of new bands that correspond to the neat organic linker that are not seen in the other samples at 1680, 1296, 1137, 1110, 940, and 733 cm^{-1}. Furthermore, a decrease in the intensity at 1653 and 1428 cm^{-1}, corresponding to the carboxylate asymmetric and symmetric stretch respectively, along with the appearance of bands at 1680 and 1296 cm^{-1}, corresponding to the C=O stretch and C–OH combination band of a carboxylic acid respectively, indicate a transformation of the ZrMOF–BDC carboxylate groups to their protonated analogs. Chloride ions in solution may provide charge compensation to the structure, as seen in Scheme 1. The reversibility of this scheme makes the structural breakdown incomplete due to the need to break four Zr–O bonds between each organic linker with two $Zr_6O_4(OH)_4$ SBUs.

ZrMOF–BDC exposed to NaOH exhibits a dramatic change in its FTIR spectrum. The only stretches in the FTIR spectra are broad and weak in intensity at 1573, 1352, 1092, 1058, 950, 850, and 757 cm^{-1}. These bands are similar to those found in neat $Zr(OH)_4$, as seen in Fig. S5.† These results are consistent with those found by Kandiah *et al.*, in which strong bases have the ability to break apart the structure of ZrMOF–BDC and ZrMOF–NH_2.[17] Furthermore, the solubility of the organic linkers in basic solutions would leave it in solution upon vacuum filtration, and no evidence of it in the FTIR pattern of the resulting powder.[22] It would be expected that the $Zr_6O_4(OH)_4$ SBU has very similar chemical properties to those of zirconium carbonates at the connection between the SBU and organic linker. It has been seen by others that zirconium carbonates can be used to form zirconium hydroxide polymorphs.[30] A proposed scheme for the breaking apart of the ZrMOF structure by NaOH is presented in Scheme 2. This reaction is presumed to go to near completion as there are no bands from the residual organic linker in the FTIR pattern. It would be expected that the SBUs may condense with one another to form larger polymorphs, as is typical for zirconium hydroxide.[28]

ZrMOF–NH_2 shows similar stability to ZrMOF–BDC, with the exception of not having the protonation of the carboxyl group upon exposure to HCl. This increase in stability towards HCl is likely due to a combination of steric and electronic effects. The –NH_2 groups of ZrMOF–NH_2 block guest molecules from easily accessing the carboxylate groups and subsequently breaking Zr–O bonds. Furthermore, the carboxylate groups are protected by the pendant –NH_2 groups from HCl through the formation of a –$NH_3^+Cl^-$ adduct. Lastly, the higher pK_a of the carboxylic acid groups of the 2-aminoterephthalic acid linker compared to 1,4-benzene dicarboxylic acid through induction leads to stronger Zr–O bonds between the SBU and the carboxylate groups. NaOH exposed ZrMOF–NH_2 shows evidence of breakdown to $ZrOH_4$ similarly to NaOH exposed ZrMOF–BDC through bands at 1562, 1369, 1055, 957, 852, and 764 cm^{-1}; however, there is evidence

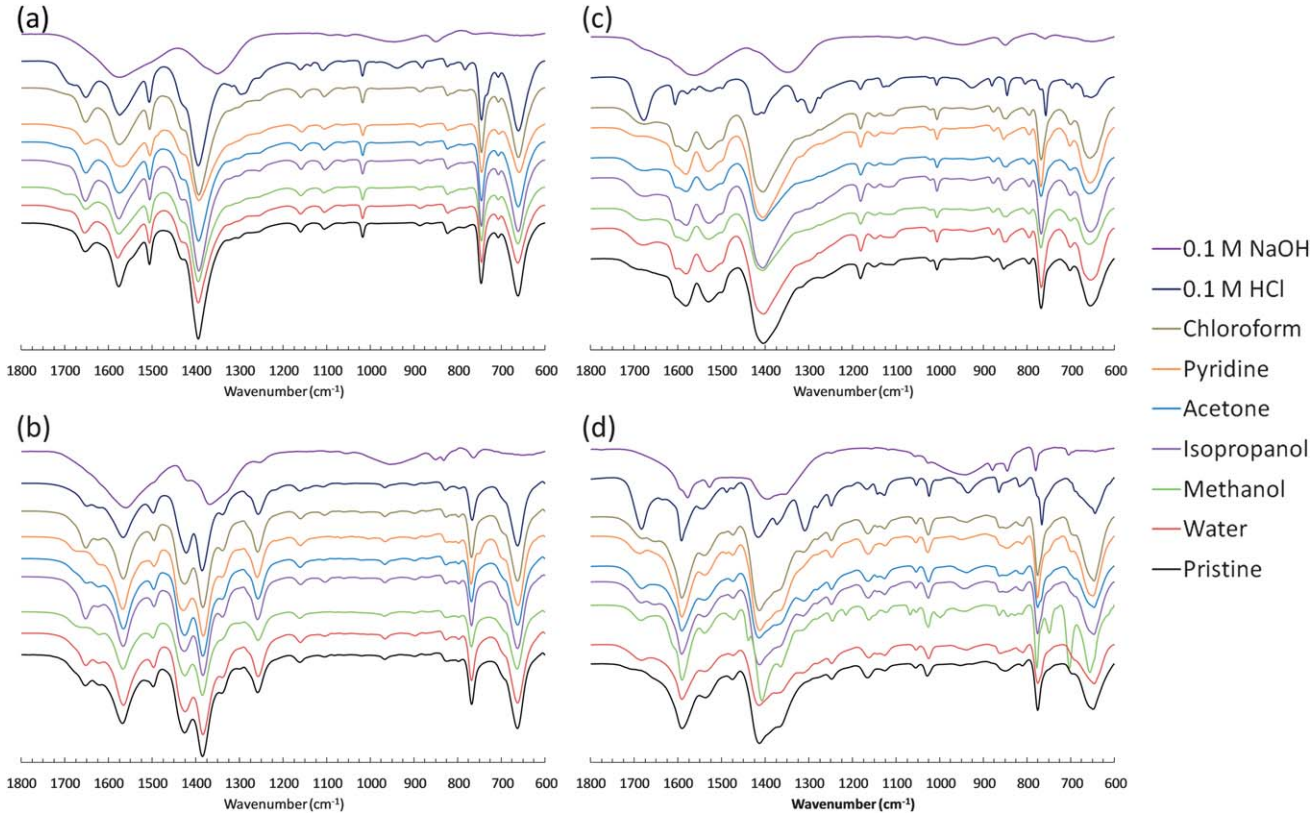

Fig. 7 ATR-FTIR spectra from 1800 to 600 cm^{-1} of (a) ZrMOF–BDC, (b) $–NH_2$, (c) –BPDC, and (d) –BIPY as synthesized and after exposure to a variety of chemicals.

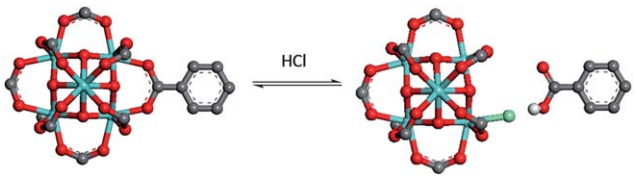

Scheme 1 The proposed mechanism for the structural breakdown of ZrMOFs in the presence of HCl. Carbon (gray), hydrogen (white), oxygen (red), zirconium (light blue), and chlorine (green) atoms can be seen; hydrogen atom are omitted for clarity.

Scheme 2 Proposed mechanism for the structural breakdown of ZrMOFs in the presence of NaOH. Carbon (gray), hydrogen (white), oxygen (red), and zirconium (light blue) atoms can be seen; hydrogen atom are omitted for clarity.

of some residual structure through bands at 1418, 1258, 832, and 764 cm^{-1}, which was not seen in ZrMOF–BDC.

ZrMOF–BPDC has IR spectra that are similar to the parent material for the samples that were exposed to water, methanol, isopropanol, acetone, pyridine, and chloroform. This is consistent with the PXRD results, except in the case of water. It is not clear as to why the IR pattern is consistent with the pristine ZrMOF–BPDC even upon structural breakdown. It appears as though the components, $Zr_6O_4(OH)_4$ and biphenyl-4,4′-dicarboxylate, each remain chemically intact but separate from one another. One possible mechanism for this occurrence can be seen in Scheme 3.

The FTIR patterns for ZrMOF–BIPY are surprisingly similar to that of the parent material, since many of the PXRD patterns showed structural breakdown. Only the FTIR patterns of HCl and NaOH showed significant change to ZrMOF–BIPY. The methanol pattern did show new bands in the Zr–O region at 748 and 705 cm^{-1}; however, there was not a significant decrease in intensity of the parent FTIR bands. There is no evidence of methyl ester formation with the organic linker in the IR pattern, meaning the new peaks must be arising from a new species formation on the SBU. These bands may be arising from the breakdown of the structure by methoxy anions that can be produced from the deprotonation of methanol by the bipyridine linker as shown in Scheme 4. Furthermore, there is no evidence

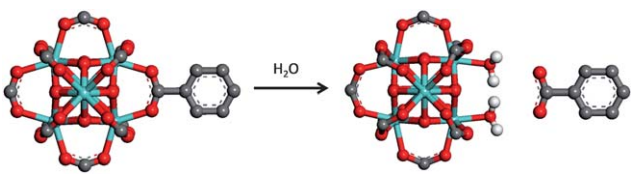

Scheme 3 Proposed mechanism for the structural breakdown of ZrMOFs in the presence of water. Carbon (gray), hydrogen (white), oxygen (red), and zirconium (light blue) atoms can be seen; hydrogen atom are omitted for clarity.

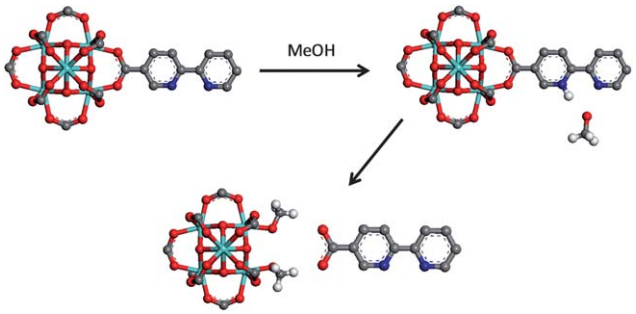

Scheme 4 Proposed mechanism for the structural breakdown of ZrMOF–BIPY in the presence of methanol *via* the production of the methoxide anion. Carbon (gray), hydrogen (white), oxygen (red), zirconium (light blue), and nitrogen (deep blue) atoms can be seen; hydrogen atom are omitted for clarity.

of a protonated form of the carboxylate through bands at approximately 1680 and 1300 cm^{-1} corresponding to the C=O stretch and C–OH combination band of a carboxylic acids.

ZrMOF–BPDC and –BIPY exhibit similar FTIR patterns upon exposure to NaOH, and show structural breakdown as seen the other ZrMOFs. For each of these structures there is evidence of some residual structure as was seen for ZrMOF–NH_2 but not ZrMOF–BDC. Furthermore the IR patterns of ZrMOF–BPDC and –BIPY upon exposure to HCl exhibit the protonation of the carboxylate group to a carboxylic acid through bands at 1686 and 1296 cm^{-1} for ZrMOF–BPDC and 1690 and 1313 cm^{-1} for ZrMOF–BIPY. When looking at the XRD patterns it is evident that the 0.1 M HCl irreversibly destroys the structure, unlike the reversible process for ZrMOF–BDC. As the process is not reversible it would be expected that a molecule of water reacts with the Zr–Cl bond in Scheme 1 to form a Zr–OH species.

The decreased stability of the double ring structures can be attributed to steric and rotational effects. Kusgens *et al.* suggested that hydrolysis of metal–carboxylate bonds in MOFs is driven by the ability of multiple water molecules to access and cluster around the metal–carboxylate sites.[8] The single ring Zr–MOFs have much narrower pores than the double ring Zr–MOFs not allowing access to the metal–carboxylate sites as well as prohibiting the organized clustering of solvent molecules to occur readily. Furthermore, the torsional barriers for biphenyl and bipyridine linkers calculated using density functional theory show local energy minima at 40° and 45° respectively and actually each shows a maximum energy at 0°, where the two rings are in the same plane.[36] Interestingly bipyridine has its overall energy minima at 180° as the interactions between the C–H of one ring and the lone pair of electrons of the nitrogen on the other ring stabilizes the structure. In the ZrMOF structure the organic linkers cannot satisfy these most stable configurations without distorting the Zr–O bonds between the $Zr_6O_4(OH)_4$ SBU and the organic linker. This distortion weakens the bonds, making them more susceptible to chemical degradation.

Conclusions

The chemical and thermal stability of the ZrMOFs can be significantly altered by the functional groups attached to as well as the length of the organic linker. ZrMOF–NH_2 has a significantly lower thermal stability likely due to the weakening of the C–C bonds between the aromatic ring and the carboxylate group due to induction. Sodium hydroxide readily breaks apart the structure of all ZrMOFs. Hydrochloric acid has the ability to reversibly protonate the carboxylate groups in ZrMOF–BDC as well as breaks apart the structure of the double ring systems of ZrMOF–BPDC and –BIPY. ZrMOF–BPDC and –BIPY are also unstable to liquid water and water vapor as was determined through PXRD and nitrogen isotherm measurements respectively. The instability of biphenyl ring derivative ZrMOFs can best be explained by the torsional strain that is experienced in the crystalline structure, making the ZrMOFs more susceptible to structural breakdown. ZrMOF–BIPY is the least chemically stable of the ZrMOFs, as the bipyridine group has the ability to deprotonate protic molecules creating strong nucleophiles that can break apart the $Zr_6O_4(OH)_4$ SBU. Furthermore, we determined that multiple techniques must be used to determine the complete chemical stability of MOFs, as we were able to determine vital information for the mechanisms of chemical breakdown from a combination of water vapor and nitrogen isotherms, PXRD, and FTIR.

Acknowledgements

The authors thank the Defense Threat Reduction Agency for funding under project number BA07PRO104.

References

1 B. Xiao, P. S. Wheatley, X. Zhao, A. J. Fletcher, S. Fox, A. G. Rossi, I. L. Megson, S. Bordiga, L. Regli, K. M. Thomas and R. E. Morris, *J. Am. Chem. Soc.*, 2007, **129**, 1203–1209.
2 U. Mueller, M. Schubert, F. Teich, H. Puetter, K. Schierle-Arndt and J. Pastre, *J. Mater. Chem.*, 2006, **16**, 626–636.
3 Y. Cui, Y. Yue, G. Qian and B. Chen, *Chem. Rev.*, 2011, **112**, 1126–1162.
4 L. E. Kreno, K. Leong, O. K. Farha, M. Allendorf, R. P. Van Duyne and J. T. Hupp, *Chem. Rev.*, 2011, **112**, 1105–1125.
5 T. G. Glover, G. W. Peterson, B. J. Schindler, D. Britt and O. Yaghi, *Chem. Eng. Sci.*, 2011, **66**, 163–170.
6 G. W. Peterson, G. W. Wagner, A. Balboa, J. Mahle, T. Sewell and C. J. Karwacki, *J. Phys. Chem. C*, 2009, **113**, 13906–13917.
7 M. Eddaoudi, J. Kim, N. Rosi, D. Vodak, J. Wachter, M. O'Keeffe and O. M. Yaghi, *Science*, 2002, **295**, 469–472.
8 P. Küsgens, M. Rose, I. Senkovska, H. Fröde, A. Henschel, S. Siegle and S. Kaskel, *Microporous Mesoporous Mater.*, 2009, **120**, 325–330.
9 K. Tan, N. Nijem, P. Canepa, Q. Gong, J. Li, T. Thonhauser and Y. J. Chabal, *Chem. Mater.*, 2012, **24**, 3153–3167.
10 J. B. Decoste, G. W. Peterson, M. W. Smith, C. A. Stone and C. R. Willis, *J. Am. Chem. Soc.*, 2012, **134**, 1486–1489.
11 S. J. Yang and C. R. Park, *Adv. Mater.*, 2012, **24**, 4010–4013.
12 H. Li, W. Shi, K. Zhao, H. Li, Y. Bing and P. Cheng, *Inorg. Chem.*, 2012, **51**, 9200–9207.

13 H. Jasuja, Y.-g. Huang and K. S. Walton, *Langmuir*, 2012, **28**, 16874–16880.
14 H. Jasuja, N. C. Burtch, Y.-g. Huang, Y. Cai and K. S. Walton, *Langmuir*, 2012, **29**, 633–642.
15 J. H. Cavka, S. Jakobsen, U. Olsbye, N. Guillou, C. Lamberti, S. Bordiga and K. P. Lillerud, *J. Am. Chem. Soc.*, 2008, **130**, 13850–13851.
16 S. Chavan, J. G. Vitillo, D. Gianolio, O. Zavorotynska, B. Civalleri, S. Jakobsen, M. H. Nilsen, L. Valenzano, C. Lamberti, K. P. Lillerud and S. Bordiga, *Phys. Chem. Chem. Phys.*, 2012, **14**, 1614–1626.
17 M. Kandiah, M. H. Nilsen, S. Usseglio, S. Jakobsen, U. Olsbye, M. Tilset, C. Larabi, E. A. Quadrelli, F. Bonino and K. P. Lillerud, *Chem. Mater.*, 2010, **22**, 6632–6640.
18 A. Schaate, P. Roy, A. Godt, J. Lippke, F. Waltz, M. Wiebcke and P. Behrens, *Chem.–Eur. J.*, 2011, **17**, 6643–6651.
19 S. J. Garibay and S. M. Cohen, *Chem. Commun.*, 2010, **46**, 7700–7702.
20 H. Jasuja, J. Zang, D. S. Sholl and K. S. Walton, *J. Phys. Chem. C*, 2012, **116**, 23526–23532.
21 Y. Huang, W. Qin, Z. Li and Y. Li, *Dalton Trans.*, 2012, **41**, 9283–9285.
22 M. Kim, J. F. Cahill, Y. Su, K. A. Prather and S. M. Cohen, *Chem. Sci.*, 2012, **3**, 126–130.
23 M. Kim and S. M. Cohen, *CrystEngComm*, 2012, **14**, 4096–4104.
24 M. Kim, J. F. Cahill, H. Fei, K. A. Prather and S. M. Cohen, *J. Am. Chem. Soc.*, 2012, **134**, 18082–18088.
25 K. E. deKrafft, W. S. Boyle, L. M. Burk, O. Z. Zhou and W. Lin, *J. Mater. Chem.*, 2012, **22**, 18139–18144.
26 E. D. Bloch, D. Britt, C. Lee, C. J. Doonan, F. J. Uribe-Romo, H. Furukawa, J. R. Long and O. M. Yaghi, *J. Am. Chem. Soc.*, 2010, **132**, 14382–14384.
27 K. S. Walton and R. Q. Snurr, *J. Am. Chem. Soc.*, 2007, **129**, 8552–8556.
28 J. A. Navio, G. Colon, P. J. SanchezSoto and M. Macias, *Chem. Mater.*, 1997, **9**, 1256–1261.
29 G. W. Peterson, J. A. Rossin, C. J. Karwacki and T. G. Glover, *J. Phys. Chem. C*, 2011, **115**, 9644–9650.
30 P. D. Southon, J. R. Bartlett, J. L. Woolfrey and B. Ben-Nissan, *Chem. Mater.*, 2002, **14**, 4313–4319.
31 P. M. Schoenecker, C. G. Carson, H. Jasuja, C. J. J. Flemming and K. S. Walton, *Ind. Eng. Chem. Res.*, 2012, **51**, 6513–6519.
32 A. D. Wiersum, E. Soubeyrand-Lenoir, Q. Yang, B. Moulin, V. Guillerm, M. Ben Yahia, S. Bourrelly, A. Vimont, S. Miller, C. Vagner, M. Daturi, G. Clet, C. Serre, G. Maurin and P. L. Llewellyn, *Chem.–Asian J.*, 2011, **6**, 3270–3280.
33 G. Suárez, Y. Sakka, T. Suzuki, T. Uchikoshi and E. F. Aglietti, *Mater. Res. Bull.*, 2009, **44**, 1802–1805.
34 L. Valenzano, B. Civalleri, S. Chavan, S. Bordiga, M. H. Nilsen, S. Jakobsen, K. P. Lillerud and C. Lamberti, *Chem. Mater.*, 2011, **23**, 1700–1718.
35 F. Márquez, I. L. Tocón, J. C. Otero and J. I. Marcos, *J. Mol. Struct.*, 1997, **410–411**, 447–450.
36 A. Göller and U.-W. Grummt, *Chem. Phys. Lett.*, 2000, **321**, 399–405.

